Geophysical Research Letters

RESEARCH LETTER
10.1029/2018GL079006

MMS Observations of Harmonic Electromagnetic Ion Cyclotron Waves

M. E. Usanova[1], N. Ahmadi[1], D. M. Malaspina[1], R. E. Ergun[1], K. J. Trattner[1], Q. Reece[1,2], T. Leonard[1], S. A. Fuselier[3,4], R. B. Torbert[5], C. T. Russell[6], and J. L. Burch[3]

[1]Laboratory for Atmospheric and Space Physics, University of Colorado Boulder, Boulder, CO, USA, [2]Boulder High School, Boulder, CO, USA, [3]Southwest Research Institute, San Antonio, TX, USA, [4]Department of Physics and Astronomy, University of Texas at San Antonio, San Antonio, TX, USA, [5]Space Science Center, University of New Hampshire, Durham, NH, USA, [6]Institute of Geophysics and Planetary Physics, University of California, Los Angeles, CA, USA

Abstract Harmonically related electromagnetic ion cyclotron waves with the fundamental frequency near the double oxygen cyclotron frequency were observed by the MMS spacecraft on 18–20 May 2016. The wave activity lasted for three days, detected by the spacecraft on their consecutive inbound passages through the Earth's plasma sheet boundary layer. The waves were seen in both magnetic and electric fields, formed by over 10 higher order harmonics. Simultaneous ion flux measurements show the presence of ion ring distributions suggesting the energy source for the observed waves. The ion cyclotron harmonics were observed together with broadband waves extending from ~Hz to ~kHz frequency range, ion and electron phase space holes, and chorus waves. During some intervals, there is a clear modulation of chorus wave packets at the ion cyclotron fundamental harmonic frequency. These observations are particularly interesting since they suggest cross-frequency and cross-species coupling between processes happening on ion and electron scales.

Plain Language Summary We presented an example oxygen harmonic wave event observed by the MMS spacecraft in the morning magnetosphere. The observed harmonic waves are transverse electromagnetic and propagate almost parallel to the background magnetic field at lower harmonics and become electrostatic at higher harmonics. Energetic ion measurements show enhanced approximately a few keV H^+ and O^+ fluxes and the presence of H^+ and O^+ ring distributions suggesting that the wave energy source for the observed waves is provided by these distributions. Harmonics were accompanied by higher frequency broadband waves extending from ~Hz to ~kHz frequency range, ~ms spikes in the electric field and chorus waves. The latter were modulated at the fundamental frequency of the ion cyclotron harmonic wave. These observations are particularly interesting since they suggest cross-frequency and cross-species coupling between kinetic plasma processes happening on ion and electron scales.

Key Points:
- Harmonic ion cyclotron waves with the fundamental frequency near the double oxygen cyclotron frequency were observed in the plasma sheet boundary layer
- The presence of H^+ and O^+ ring distributions suggests that the wave energy source for the observed waves is provided by these distributions
- There is a clear modulation of simultaneously observed chorus wave packets at the ion cyclotron fundamental harmonic frequency

Supporting Information:
- Supporting Information S1

Correspondence to:
M. E. Usanova,
maria.usanova@lasp.colorado.edu

Citation:
Usanova, M. E., Ahmadi, N., Malaspina, D. M., Ergun, R. E., Trattner, K. J., Reece, Q., et al. (2018). MMS observations of harmonic electromagnetic ion cyclotron waves. *Geophysical Research Letters*, *45*, 8764–8772. https://doi.org/10.1029/2018GL079006

Received 14 JUN 2018
Accepted 2 AUG 2018
Accepted article online 6 AUG 2018
Published online 12 SEP 2018

1. Introduction

Harmonic electromagnetic ion cyclotron waves have been observed in various regions of the Earth's magnetosphere: the inner magnetosphere (e.g., Fraser et al., 1996), plasma sheet boundary layer (PSBL; Broughton et al., 2008), upward current regions of the auroral oval (e.g., Chaston et al., 2002; Santolik et al., 2002), and equatorial ionosphere (Parrot et al., 2006). In most reported cases these waves propagate almost perpendicular to the background magnetic field, **B**, have their energy source in ion ring distributions (i.e., $\partial f/\partial v_\perp > 0 : v_\parallel = 0$) and grow from ion Bernstein instability (e.g., Gary et al., 2010). In the PBSL, the harmonic wave fundamental frequency lies in the vicinity of the local proton (H^+) cyclotron frequency, while in the inner magnetosphere it can also be generated close to the cyclotron frequency of minor ion species, He^+ and O^+. In the auroral zone, electromagnetic proton harmonic waves can grow through inverse Landau resonance with a cold electron beam (e.g., Chaston et al., 2002).

Occurrence distribution and properties of ion cyclotron harmonics depend on the magnetospheric region where they are observed. In the PSBL, they are predominately perpendicular propagating, having dominant fluctuations (order of 1 nT in magnetic field and 1 mV/m in electric field) transverse to the background magnetic field. Statistical studies by Broughton et al. (2008) and Engebretson et al. (2010) showed that proton harmonic waves were observed in 30% of Cluster satellite crossings of the PSBL.

In the inner magnetosphere, proton harmonic waves can be both compressional and Alfvénic. For example, GEOS spacecraft observations by Perraut et al. (1982) show that proton harmonic waves are often generated in the equatorial magnetosphere (L = 4–8) with amplitude ~0.01–0.1 nT directed along the background magnetic field. The wave activity typically lasts from tens of minutes to hours and its occurrence peaks at ~30% in the afternoon sector. Further developed theory showed that these compressional waves are fast magnetosonic waves (Horne & Thorne, 1998; Meredith et al., 2008). Similar to the harmonic waves generated in the PSBL, they are generated by ring distributions of $5 \lesssim E \lesssim 30$ keV protons (Perraut et al., 1982). Though the source of free energy for both compressional and Alfvénic harmonic waves is provided by proton ring velocity distributions, ion beta controls the character of the instability: for beta of order unity the instability is transverse electromagnetic, while for increasing ion beta it becomes compressional (Denton et al., 2010).

Ion cyclotron harmonic waves with fundamental frequency near the helium or oxygen cyclotron frequency are reported more rarely than proton harmonics and their observations are limited to the inner magnetosphere and are specific to geomagnetically active times. They are observed in a wide range of L-shells and magnetic local times. Helium and oxygen harmonics were observed by the Akebono satellite in the equatorial plasmasphere at L ~ 1.5–2.5 and ~2–18 MLT (Kokubun et al., 1991 and Liu et al., 1994). The helium harmonics had a dominant component along the background magnetic field and left-handed polarization in the plane perpendicular to the background magnetic field. Liu et al. (1994) reported highly oblique oxygen harmonic waves propagating at phase velocity much less than the Alfvén velocity. The distinctive feature of these waves is that they were observed in the morning magnetosphere during intense magnetic storms ($Dst < -100$ nT) suggesting that energetic ring current oxygen ions typical to the main storm phase provided a source of free energy for the detected waves. These Akebono observations were further explained by Pokhotelov et al. (1997) (Pokhotelov et al., 1998). Their analytical model demonstrated that the source of free energy for the harmonic emissions can be provided by loss cone or ring distributions of hot ions with a distribution function having a positive slope $\partial f/\partial v_\perp > 0$ and that the instability growth rate, γ, is proportional to the number density of the hot ions and also controlled by a number of cold oxygen ions, n_{O^+} with $\gamma \propto \sqrt{n_{O^+}}$. Analysis of Cluster ion data by Kronberg et al. (2012) showed that enhanced oxygen fluxes are typically observed in the magnetosphere during disturbed geomagnetic conditions.

Fraser et al. (1996), Ukhorskiy et al. (2010), and Usanova et al. (2016) showed that electromagnetic ion harmonic waves can also be parallel propagating in the inner magnetosphere. However, these waves often have mixed polarization and varying ellipticity, which may be indicative of the superposition of many linearly polarized waves in the plane perpendicular to **B** (Santolik et al., 2002). Lee and Lee (2016) investigated mechanisms for this wave excitation in the magnetosphere and concluded that anisotropic oxygen bunch distributions can excite harmonic waves with fundamental frequency between He^+ and O^+ gyrofrequencies that can propagate at various directions, from parallel to quasi-perpendicular. A recent analysis by Min et al. (2017) suggests that the ion Bernstein instability may be a possible source for harmonic waves reported by Usanova et al. (2016), but further self-consistent numerical modeling is crucial for testing this theory.

Proton harmonic waves have been often observed together with higher frequency waves. First, the parallel component of the harmonic wave electric field often contains short-lived (approximately a few millisecond) bipolar electric field structures known as electron phase space holes (Chaston et al., 2002). These structures are formed on a microscale in plasma regions where the electron density is lower than the surrounding plasma and can be observed in different plasma environments including the auroral zone and plasma sheet (see, e.g., Andersson et al., 2009; Ergun et al., 1998). Second, ion cyclotron harmonics are often associated with broadband waves covering a wide range of frequencies from DC up to a few harmonics of proton cyclotron frequency. These waves can be generated by the electron beam-plasma instability and become more pronounced with increasing cold plasma density (Chaston et al., 2002). In addition, broadband electrostatic waves extending up to 4 kHz are often observed in PSBL in association with 3–100 keV ion beamlets (Keiling et al., 2006). These waves were proposed to be driven by ion shell distributions (Olsson et al., 2004). Though Olsson et al. (2004) and Keiling et al. (2006) did not report direct observations of ion cyclotron harmonics, the latter may potentially be related to broadband electrostatic waves through the same energy source.

Colpitts et al. (2016) presented observations of various higher frequency waves including broadband (~50–2,500 Hz) waves, whistler mode chorus and hiss waves, and magnetosonic waves modulated at the frequency of co-located ion harmonic waves in the inner magnetosphere. Such modulation may indicate cross-scale

coupling involving nonlinear interactions between the ion and electron cyclotron wave modes that could significantly impact wave-particle interactions such as acceleration and pitch angle scattering (Colpitts et al., 2016).

In this letter, we report first MMS observations of harmonically related electromagnetic ion cyclotron waves simultaneously with electron and ion phase space holes and modulation of higher frequency chorus wave growth in the PSBL. We also provide a detailed analysis of ion velocity distributions over the entire interval of wave observations.

2. Instrumentation

Magnetospheric Multiscale (MMS) is a National Aeronautics and Space Administration (NASA) satellite mission launched on 12 March 2015 that consists of four identical spacecraft in similar orbits with varying satellite separation. The primary focus of this mission is to investigate kinetic plasma processes during magnetic reconnection, in both the dayside and nightside magnetosphere (Burch et al., 2016). Hence, the spacecraft traverse the entire magnetosphere with their orbit apogee near expected reconnection sites, at 12 Re on the dayside and 25 Re in the tail. For this study, we used 3-D measurements of magnetic and electric fields from the FIELDS instrument. The FIELDS magnetic sensors consist of flux-gate magnetometers (AFG and DFG) providing measurements over the frequency range from DC to 64 Hz and a search coil magnetometer (SCM) covering the full whistler mode spectrum (Le Contel et al., 2014; Russell et al., 2014). The FIELDS three-axis electric field measurements are provided by two sets of double-probe spin-plane and axial sensors (SDP and ADP) at varying cadence depending on the location of region of interest (Ergun et al., 2016; Lindqvist et al., 2014; Torbert et al., 2016). The Hot Plasma Composition Analyzer (HPCA) data were used to look at 1 eV–40 keV ion velocity distributions (Young et al., 2016). Due to low ion count rates in the region of interest, we used survey-mode data averaged over 1 min for H^+ and 4 min for the O^+ ions. The He^+ fluxes were negligible during the event so we assume that He^+ did not play a significant role in the observed processes.

3. Observations

3.1. Solar Wind and Geomagnetic Conditions

Ion cyclotron harmonic waves were observed by the four MMS probes during an interval of prolonged relatively quiet geomagnetic conditions in a late storm recovery phase (as indicated by the Sym-H index). The wave activity was sustained over the course of three days, between 18 and 20 May when the spacecraft traversed the same region of the morning magnetosphere at L ~ 9 and MLT ~ 4. Solar wind characteristics (interplanetary magnetic field Bz, flow speed, density, and dynamic pressure) and geomagnetic indices (AE and Sym-H) from 18 to 21 May exhibited some variations (Figure S1 in the supporting information). There were multiple negative excursions in the interplanetary magnetic field Bz during this interval. The solar wind speed was steadily decreasing from ~500 to 450 km/s; the proton density fluctuated between ~1.5 and 11 n/cc, which resulted in several enhancements of solar wind dynamic pressure up to ~4 nPa. Geomagnetic conditions were somewhat disturbed at the beginning of this three-day interval where the AE index reached ~800 nT and Sym-H dropped down to −30 nT; however, later they remained pretty calm.

3.2. Wave Properties

In this section, we focus on simultaneous observations of cyclotron harmonic and higher frequency VLF waves from 19:00 to 20:45 UT on 20 May 2016. Figure 1 shows spectrograms of the magnetic (a) and electric (b) field in GSE coordinates. The white curves in each panel denote the local oxygen, helium, and hydrogen gyrofrequencies. Magnetic field measurements show predominately the lowest frequency harmonic at twice the oxygen gyrofrequency. During a short period of time, just before 20:00 UT a higher number of harmonics are observed, though those are not very pronounced. On the other hand, electric field measurements clearly show over 10 harmonics extending to slightly above the hydrogen gyrofrequency. These observations are consistent with Chaston et al. (2002) demonstrating that harmonic waves become more electrostatic with increasing frequency. Figure 1c shows the omnidirectional dynamic spectra of high-frequency electric field. The upper-band chorus waves and broadband wave activity is clearly present between 19:00 and 20:00 UT, partially overlapping the interval of harmonic wave observations. At the times marked by the vertical magenta lines, there was also electric field burst data available. A detailed analysis of these high-resolution measurements will be presented in section below.

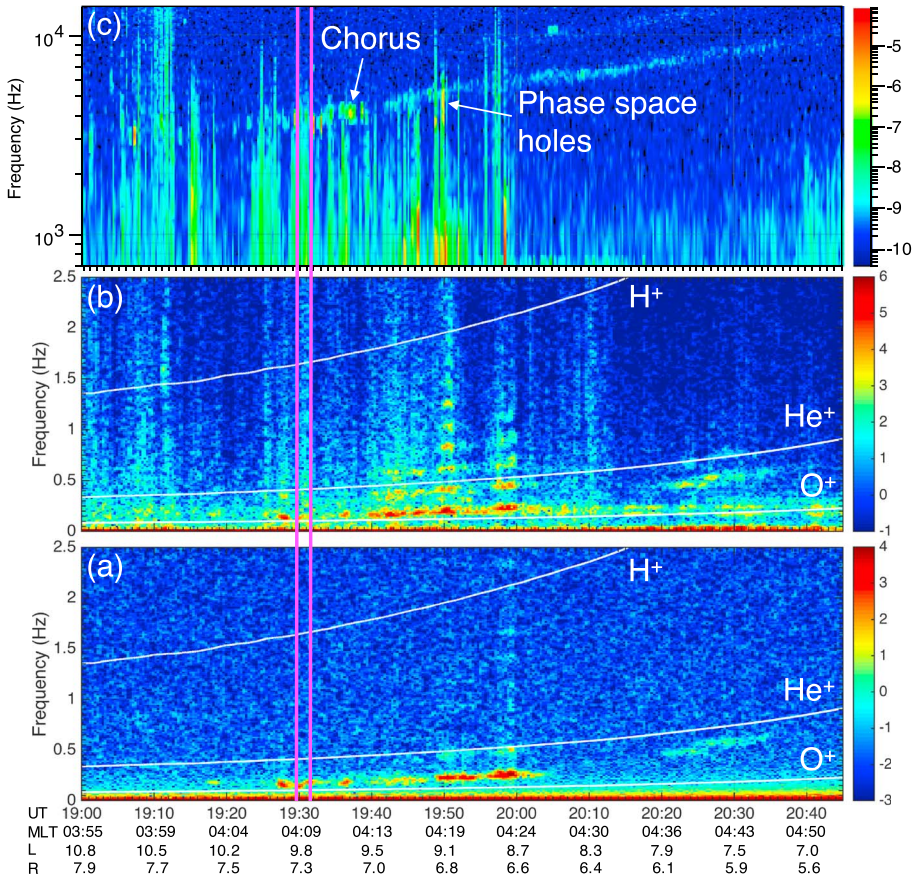

Figure 1. Fast Fourier transform spectrograms of (a) the ultra-low-frequency Bx_{GSE} magnetic field component, (b) the ultra-low-frequency Ex_{GSE} electric field component between 0 and 2.5 Hz, (c) the VLF omni-directional electric field between 592 and 65.5 kHz. The white curves in panels (a) and (b) show the local H^+, He^+, and O^+ ion gyrofrequencies. The vertical magenta lines denote the interval of high-frequency wave observations shown in Figure 3.

For a more in-depth wave analysis, we first converted the three components of electric and magnetic field data from GSE into magnetic field-aligned coordinates. Electric field data (32 samples/s) were linearly interpolated into the magnetic field data cadence (16 samples/s). The background magnetic field vector was defined using smoothed (1-min sliding boxcar averages) of the GSE magnetic field components. To look at the wave properties, we applied a Morlet-wavelet transform in the same way as Usanova et al. (2016). The advantage of using wavelets compared to fast Fourier transform is that they provide varying resolution at low and high frequencies, being suitable for analysis of nonstationary signals with a superposition of multiple harmonics.

Wave characteristics were determined using the singular value decomposition (SVD) method (Santolík et al., 2003). The wave properties observed here are very similar to those reported by Usanova et al. (2016). Figure 2 shows magnetic field spectrograms of the parallel (a) and perpendicular (b) magnetic field components in field-aligned coordinates. The local oxygen and helium gyrofrequencies are shown by the white curves. The waves are predominately transverse at lower harmonics and become electrostatic at higher harmonics. Panels (c–f) show the wave properties: ellipticity (c), wave normal angle (d), the parallel Poynting flux (e), and the angle of energy propagation with respect to the background magnetic field (f). The waves have mixed positive and negative ellipticity and propagate at a small wave normal angle to the background magnetic field. The wave energy propagates almost parallel and bidirectionally, which implies that the waves were detected in their source region (e.g., Loto'aniu et al., 2005). Interestingly, the energy of the isolated He-band EMIC waves observed after 20:20 UT propagates unidirectionally indicating that those waves were not locally generated.

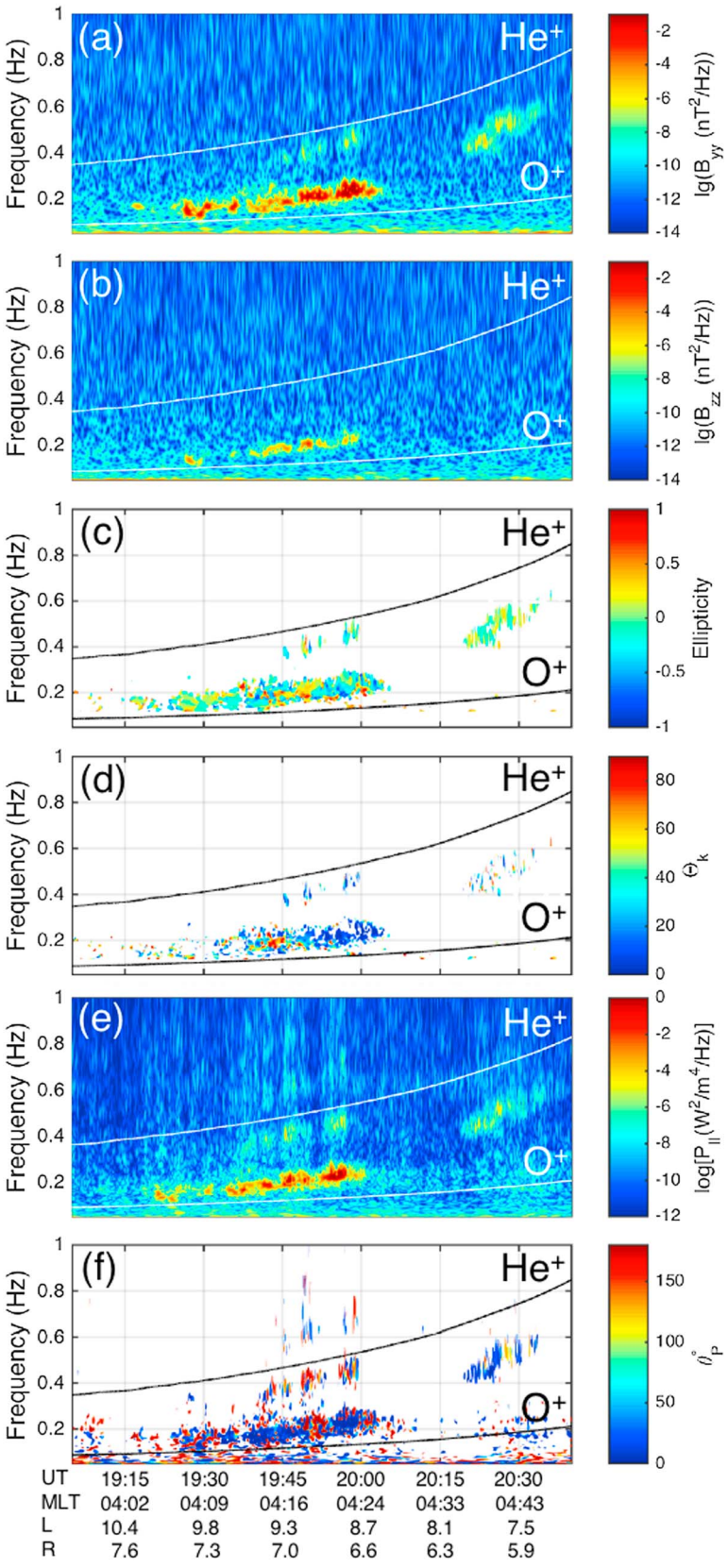

Figure 2. Harmonic wave properties: (a and b) power spectral density of the perpendicular (By) and parallel (Bz) magnetic field component, (c) ellipticity (blue, left-hand; red, right-hand), (d) wave normal angle, (e) parallel Poynting flux, and (f) angle between the Poynting flux and **B**.

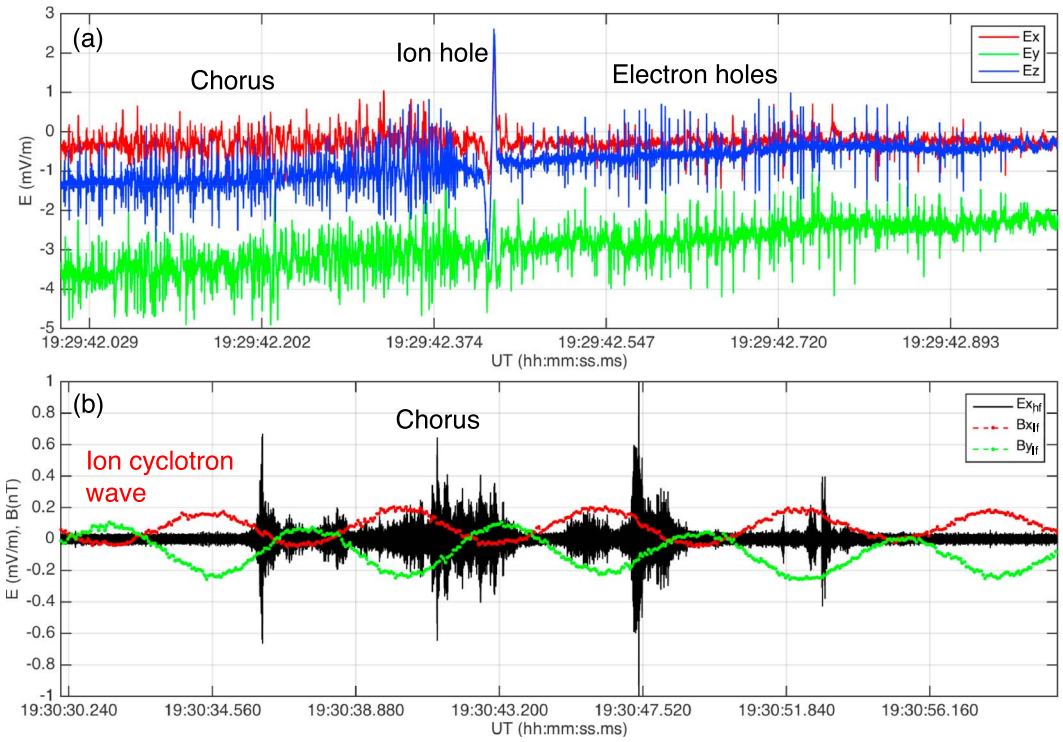

Figure 3. High-resolution electric field measurements in field-aligned coordinates. (a) Parallel (blue) and two perpendicular (red and green) components of electric field between 19:29:42 and 19:29:43 UT. (b) Perpendicular component of chorus wave electric field (black curve) and two perpendicular components of ion harmonic wave magnetic field (red and green curves) between 19:30:30 and 19:31:00 UT. Chorus wave packets are modulated at the fundamental ion cyclotron wave frequency.

3.3. Low- and High-Frequency Waves

In this section, we focus on the analysis of high-resolution (16,384 samples/s) electric field burst data during two intervals. Events occurred during both intervals were observed together with the cyclotron harmonic wave activity. Figure 3a shows three components of electric field in field-aligned coordinates from 19:29:42 to 19:29:43 UT (the blue, and the red and green colors denote the parallel and two perpendicular components, respectively). This interval demonstrates a clear transition between three types of phenomena happening on a subsecond scale: chorus waves at the beginning and electron phase space holes at the end of the interval, separated by an ion hole. The electron and ion phase space holes are characterized by isolated bipolar spikes in the parallel electric field lasting a few milliseconds. The ion hole can be distinguished from electron holes by the opposite polarity (due to opposite charge), larger amplitude, and longer duration. Kinetic Vlasov simulations by Main et al. (2006) showed that ion phase space holes can be driven by a relative drift between H^+ and O^+ ions. Since increased fluxes of both species are present during this interval, this mechanism may be responsible for the ion hole formation.

Figure 3b shows two perpendicular components of ultra-low-frequency magnetic field (Bx_{lf} and By_{lf}; the red and green curves) and one perpendicular electric field component (Ex_{hf}; the black curve) in field-aligned coordinates from 19:30:30 to 19:31:00 UT. A closer look at this 30-s interval shows that the chorus wave packets have the same repetition frequency as the fundamental frequency of the ion cyclotron harmonic waves.

The modulation of chorus and the intensification of phase space holes detected simultaneously with ion cyclotron harmonics are particularly interesting since they further support the hypothesis that processes occurring on ion and electron scales maybe related, potentially through nonlinear coupling.

3.4. Ion Velocity Distributions

We examined high-resolution ion measurements and looked at the evolution of the H^+ and O^+ ion velocity distributions to pinpoint the source of energy for the ion cyclotron harmonic waves. The He^+ fluxes were

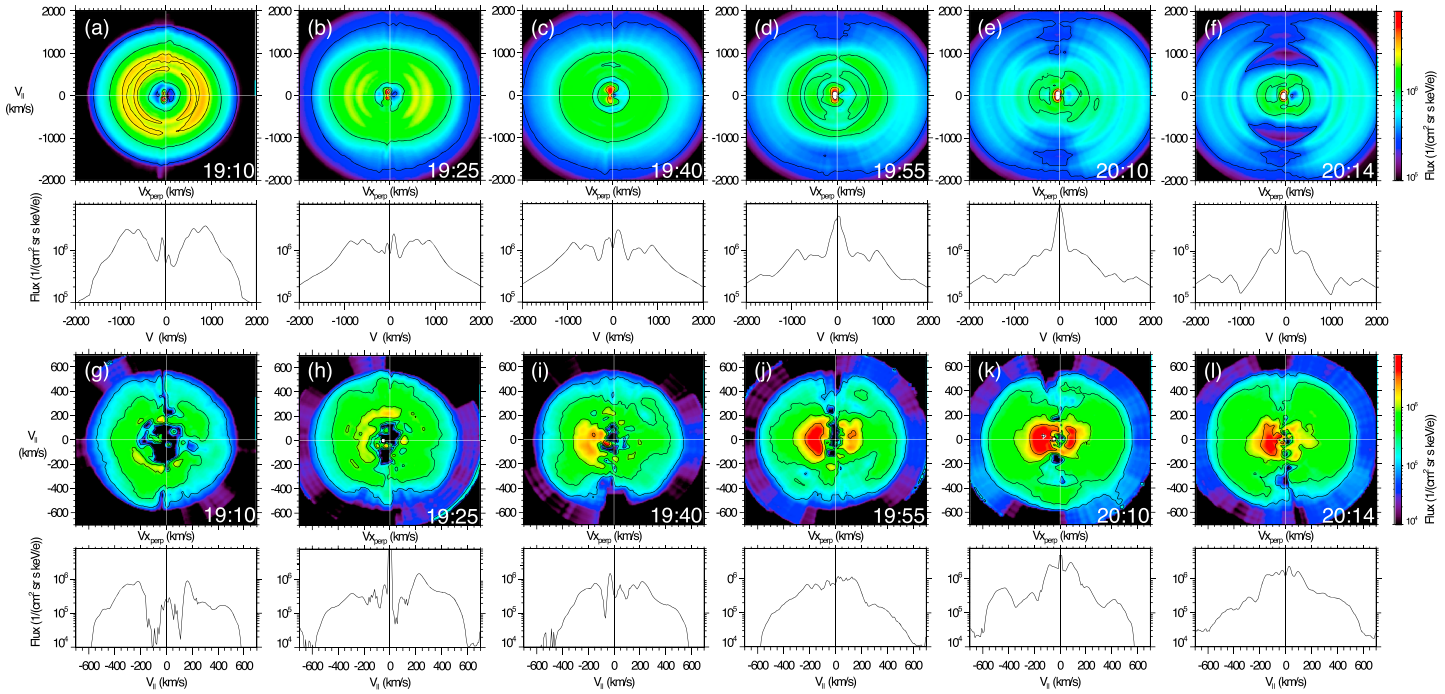

Figure 4. (a–f) H^+ and (g–l) O^+ ion velocity distributions in field-aligned coordinate system. Color-coded is the ion flux plotted on a log-scale. The bottom panels show a cut through the distribution along the magnetic field direction.

low throughout the entire event so we assume that they did not play a significant role in wave generation. The wave activity was associated with the increase in a few keV H^+ and O^+ ion fluxes. The density went up from 1.6 to 2.3 n/cc and from 0.005 to 0.03 n/cc for H^+ and O^+, respectively (not shown here).

Figure 4 shows H^+ and O^+ ion velocity distributions in the field-aligned coordinate system (with the perpendicular bulk velocity removed) between 19:00 and 20:14 UT when HPCA data were available. The bottom panels show a cut through the distribution along the magnetic field direction. For conversion into field-aligned coordinate system, we use measurement points within a ±45-degree pie-shaped slice around the *x*-*z* plane (where *z* is along **B**; *x* and *y* are the two perpendicular directions) and rotate them into the plane by conserving pitch angle and energy. The other ±45-degree slice is rotated into the *y*-*z* plane. Each 10-s data segment contains more than 16,000 measurements, which are averaged over 1 min for the H^+ and 4 min for the O^+ ions.

The velocity distribution is generally consistent with the observations by Fennell et al. (1981; their Figure 3) where the cold and the hot ion populations exhibit different behavior. The cold hydrogen component is field-aligned, indicative of the ionospheric source. On the other hand, the hot hydrogen velocity distribution has a double-ring structure, which evolved throughout the entire wave observation interval. Such structures have been observed in the PSBL (e.g., Saito et al., 1994). At 19:10 UT, just before the wave activity onset, the distribution was isotropic, having two maxima at ~550 km/s (2.9 keV) and 900 km/s (4.7 keV). Later, as the spacecraft moved inward and the wave activity progressed, the distribution became anisotropic, elongated in the perpendicular direction and the rings increased in both size and number. Generally, the O^+ distributions followed the same trend, though the multiring structure was not as pronounced as in the case of hydrogen, perhaps due to lower fluxes and resulting noise.

Chen et al. (2010) analyzed conditions leading to generation of ion Bernstein instability and concluded that it typically occurs for $0.5 < v_r/v_A < 2$, where v_r is the ring velocity and $v_A = \sqrt{B^2/4\pi n_e m_p}$, where v_A is the Alfven speed, B is the background magnetic field, n_e is the background electron density, and m_p is the proton mass. For the plasma parameters observed during this event, that is, B = 130 nT, n_e = 2 cm^{-3}, the Alfven speed v_A = 640 km/s, and the ratio v_r/v_A falls into the range unstable to ion Bernstein mode for the proton rings

but lies outside of it for the oxygen rings. Further kinetic Vlasov theory analysis is warranted to determine the relative role of ion velocity distributions in harmonic wave generation.

4. Summary and Conclusions

We presented an example oxygen cyclotron harmonic wave event observed by the MMS spacecraft in the PSBL. The lower harmonics are transverse electromagnetic and propagate almost parallel to the background magnetic field and the higher harmonics become electrostatic. HPCA ion measurements show enhanced approximately a few keV H^+ and O^+ fluxes, and the presence of H^+ and O^+ ring distributions suggests that the wave energy source for the observed waves is provided by these distributions. The relative role of these ions species in wave generation is yet to be fully understood; hence, further kinetic Vlasov theory analysis is warranted. Harmonics were accompanied by higher frequency broadband waves extending from ~Hz to ~kHz frequency range, ion and electron phase space holes, and whistler mode chorus waves. The latter were modulated at the fundamental frequency of the ion cyclotron harmonic wave. These observations are particularly interesting since they suggest cross-frequency and cross-species coupling between kinetic processes happening on ion and electron scales. Further work will focus on examining the nonlinear temporal evolution of these waves and their self-consistent interaction with energetic ions and electrons and the role of this cross-scale coupling in the energetic particle dynamics using numerical modeling.

Acknowledgments
This work was funded by the NASA MMS project. We thank CDAWeb, SSCWeb, and Kyoto observatory for the use of their resources. We acknowledge the SCM team supported by CNES and CNRS for use of SCM data. M. E. U. would like to thank Yuri Khotyaintsev for his MATLAB code used for wave analysis and Laila Andersson for valuable discussions. M. E. U. is supported by NASA award NNX16AF91G. MMS data are publicly available and can be accessed at https://lasp.colorado.edu/mms/sdc/public/.

References

Andersson, L., Ergun, R. E., Tao, J., Roux, A., LeContel, O., Angelopoulos, V., et al. (2009). New features of electron phase space holes observed by the THEMIS mission. *Physical Review Letters*, *103*, 05990.

Broughton, M. C., Engebretson, M. J., Glassmeier, K. H., Narita, Y., Keiling, A., Fornaçon, K. H., et al. (2008). Ultra-low-frequency waves and associated wave vectors observed in the plasma sheet boundary layer by Cluster. *Journal of Geophysical Research*, *113*, A12217. https://doi.org/10.1029/2008JA013366

Burch, J. L., Moore, T. E., Torbert, R. B., & Giles, B. L. (2016). Magnetospheric multiscale overview and science objectives. *Space Science Reviews*, *199*(1-4), 5–21. https://doi.org/10.1007/s11214-015-0164-9

Chaston, C. C., Bonnel, J. W., McFadden, J. P., Ergun, R. E., & Carlson, C. W. (2002). Electromagnetic ion cyclotron waves at proton cyclotron harmonics. *Journal of Geophysical Research*, *107*(A11), 1351. https://doi.org/10.1029/2001JA900141

Chen, L., Thorne, R. M., Jordanova, V. K., & Horne, R. B. (2010). Global simulation of magnetosonic wave instability in the storm time magnetosphere. *Journal of Geophysical Research*, *115*, A11222. https://doi.org/10.1029/2010JA015707

Colpitts, C. A., Cattell, C. A., Engebretson, M., Broughton, M., Tian, S., Wygant, J., et al. (2016). Van Allen Probes observations of cross-scale coupling between electromagnetic ion cyclotron waves and higher-frequency wave modes. *Geophysical Research Letters*, *43*, 11,510–11,518. https://doi.org/10.1002/2016GL071566

Denton, R. E., Engebretson, M. J., Keiling, A., Walsh, A. P., Gary, S. P., Décréau, P. M. E., et al. (2010). Multiple harmonic ULF waves in the plasma sheet boundary layer: Instability analysis. *Journal of Geophysical Research*, *115*, A12224. https://doi.org/10.1029/2010JA015928

Engebretson, M. J., Kahlstorf, C. R. G., Posch, J. L., Keiling, A., Walsh, A. P., Denton, R. E., et al. (2010). Multiple harmonic ULF waves in the plasma sheet boundary layer observed by Cluster. *Journal of Geophysical Research*, *115*, A12225. https://doi.org/10.1029/2010JA015929

Ergun, R. E., Carlson, C. W., McFadden, J. P., Mozer, F. S., Muschietti, L., Roth, I., & Strangeway, R. J. (1998). Debye-Scale Plasma Structures Associated with Magnetic-Field-Aligned Electric Fields. *Physical Review Letters*, *81*, 826. https://doi.org/10.1103/PhysRevLett.81.826

Ergun, R. E., Tucker, S., Westfall, J., Goodrich, K. A., Malaspina, D. M., Summers, D., et al. (2016). The axial double probe and fields signal processing for the MMS mission. *Space Science Reviews*, *199*(1-4), 167–188. https://doi.org/10.1007/s11214-014-0115-x

Fennell, J. F., Croley, D. R. Jr., & Kaye, S. M. (1981). Low-energy ion pitch angle distributions in the outer magnetosphere: Ion zipper distributions. *Journal of Geophysical Research*, *86*(A5), 3375–3382. https://doi.org/10.1029/JA086iA05p03375

Fraser, B. J., Singer, H. J., Hughes, W. J., Wygant, J. R., Anderson, R. R., & Hu, Y. D. (1996). CRRES Poynting vector observations of electromagnetic ion cyclotron waves near the plasmapause. *Journal of Geophysical Research*, *101*(A7), 15,331–15,343. https://doi.org/10.1029/95JA03480

Gary, S. P., Liu, K., Winske, D., & Denton, R. E. (2010). Ion Bernstein instability in the terrestrial magnetosphere: Linear dispersion theory. *Journal of Geophysical Research*, *115*, A12209. https://doi.org/10.1029/2010JA015965

Horne, R. B., & Thorne, R. M. (1998). Potential waves for relativistic electron scattering and stochastic acceleration during magnetic storms. *Geophysical Research Letters*, *25*(15), 3011–3014. https://doi.org/10.1029/98GL01002

Keiling, A., Parks, G. K., Rème, H., Dandouras, I., Wilber, M., Kistler, L., et al. (2006). Energy-dispersed ions in the plasma sheet boundary layer and associated phenomena: Ion heating, electron acceleration, Alfvén waves, broadband waves, perpendicular electric field spikes, and auroral emissions. *Annales de Geophysique*, *24*(10), 2685–2707. https://doi.org/10.5194/angeo-24-2685-2006

Kokubun, S., Takami, M., Hayashi, K., Fukunishi, H., Kimura, I., Sawada, A., & Kasahara, Y. (1991). Triaxial search coil measurements of ELF waves in the plasmasphere: Initial results from EXOS-D. *Geophysical Research Letters*, *18*(2), 301–304. https://doi.org/10.1029/90GL02599

Kronberg, E. A., Haaland, S. E., Daly, P. W., Grigorenko, E. E., Kistler, L. M., Fränz, M., & Dandouras, I. (2012). Oxygen and hydrogen ion abundance in the near-Earth magnetosphere: Statistical results on the response to the geomagnetic and solar wind activity conditions. *Journal of Geophysical Research*, *117*, A12208. https://doi.org/10.1029/2012JA018071

Le Contel, O., Leroy, P., Roux, A., Coillot, C., Alison, D., Bouabdellah, A., et al. (2014). The search-coil magnetometer for MMS. *Space Science Reviews*, *199*(1), 257–282. https://doi.org/10.1007/s11214-014-0096-9

Lee, K. H., & Lee, L. C. (2016). Generation of He^+ and O^+ EMIC waves by the bunch distribution of O^+ ions associated with fast magnetosonic shocks in the magnetosphere. *Geophysical Research Letters*, *43*, 9406–9414. https://doi.org/10.1002/2016GL070465

Lindqvist, P.-A., Olsson, G., Torbert, R. B., King, B., Granoff, M., Rau, D., et al. (2014). The spin-plane double probe electric field instrument for MMS. *Space Science Reviews*, *199*, 137–165. https://doi.org/10.1007/s11214-014-0116-9

Liu, H., Kokubun, S., & Hayashi, K. (1994). Equatorial electromagnetic emission with discrete spectra near harmonics of oxygen gyrofrequency during magnetic storm. *Geophysical Research Letters*, *21*(3), 225–228. https://doi.org/10.1029/93GL02836

Loto'aniu, T. M., Fraser, B. J., & Waters, C. L. (2005). Propagation of electromagnetic ion cyclotron wave energy in the magnetosphere. *Journal of Geophysical Research*, *110*, A07214. https://doi.org/10.1029/2004JA010816

Main, D. S., Newman, D. L., & Ergun, R. E. (2006). Double layers and ion phase-space holes in the auroral upward-current region. *Physical Review Letters*, *97*(18), 185001. https://doi.org/10.1103/PhysRevLett.97.185001

Meredith, N. P., Horne, R. B., & Anderson, R. R. (2008). Survey of magnetosonic waves and proton ring distributions in the Earth's inner magnetosphere. *Journal of Geophysical Research*, *113*, A06213. https://doi.org/10.1029/2007JA012975

Min, K., Denton, R. E., Liu, K., Gary, S. P., & Spence, H. E. (2017). Ion Bernstein instability as a possible source for oxygen ion cyclotron harmonic waves. *Journal of Geophysical Research: Space Physics*, *122*, 5449–5465. https://doi.org/10.1002/2017JA023979

Olsson, A., Janhunen, P., & Peterson, W. (2004). Ion shell distributions as free energy source for plasma waves on auroral field lines mapping to plasma sheet boundary layer. *Annales de Geophysique*, *22*(6), 2115–2133. https://doi.org/10.5194/angeo-22-2115-2004

Parrot, M., Buzzi, A., Santolik, O., Berthelier, J. J., Sauvaud, J. A., & Lebreton, J. P. (2006). New observations of electromagnetic harmonic ELF emissions in the ionosphere by the DEMETER satellite during large magnetic storms. *Journal of Geophysical Research*, *111*, A08301. https://doi.org/10.1029/2005JA011583

Perraut, S., Roux, A., Robert, P., Gendrin, R., Sauvaud, J. A., Bosqued, J. M., et al. (1982). A systematic study of ULF waves above F_H^+ from GEOS 1 and 2 measurements and their relationships with proton ring distributions. *Journal of Geophysical Research*, *87*(A8), 6219–6236. https://doi.org/10.1029/JA087iA08p06219

Pokhotelov, O. A., Pokhotelov, D. O., Feygin, F. Z., Gladychev, V. A., Parrot, M., Hayashi, K., et al. (1997). Oxygen cyclotron harmonic waves in the deep plasmasphere during magnetic storms. *Journal of Geophysical Research*, *102*(A1), 77–83. https://doi.org/10.1029/96JA03067

Pokhotelov, O. A., Pokhotelov, D. O., Feygin, F. Z., Parrot, M., Kangas, J., Mursula, K., et al. (1998). Excitation of helium cyclotron harmonic waves during quiet magnetic conditions. *Journal of Geophysical Research*, *103*(A11), 26,585–26,593. https://doi.org/10.1029/98JA02619

Russell, C. T., Anderson, B. J., Baumjohann, W., Bromund, K. R., Dearborn, D., Fischer, D., et al. (2014). The Magnetospheric Multiscale Magnetometers. *Space Science Reviews*, *199*(1), 189–256. https://doi.org/10.1007/s11214-014-0057-3

Saito, Y., Mukai, T., Hirahara, M., Machida, S., Nishida, A., Terasawa, T., et al. (1994). GEOTAIL observation of ring-shaped ion distribution functions in the plasma sheet-lobe boundary. *Geophysical Research Letters*, *21*(25), 2999–3002. https://doi.org/10.1029/94GL02099

Santolík, O., Parrot, M., & Lefeuvre, F. (2003). Singular value decomposition methods for wave propagation analysis. *Radio Science*, *38*(1), 1010. https://doi.org/10.1029/2000RS002523

Santolik, O., Pickett, J. S., Gurnett, D. A., & Storey, L. R. O. (2002). Magnetic component of narrow-band ion cyclotron waves in the auroral zone. *Journal of Geophysical Research*, *107*(A12), 1444. https://doi.org/10.1029/2001JA000146

Torbert, R. B., Russell, C. T., Magnes, W., Ergun, R. E., Lindqvist, P.-A., LeContel, O., et al. (2016). The FIELDS instrument suite on MMS: Scientific objectives, measurements, and data products. *Space Science Reviews*, *199*, 105. https://doi.org/10.1007/s11214-014-0109-8

Ukhorskiy, A. Y., Shprits, Y. Y., Anderson, B. J., Takahashi, K., & Thorne, R. M. (2010). Rapid scattering of radiation belt electrons by storm-time EMIC waves. *Geophysical Research Letters*, *37*, L09101. https://doi.org/10.1029/2010GL042906

Usanova, M. E., Malaspina, D. M., Jaynes, A. N., Bruder, R. J., Mann, I. R., Wygant, J. R., & Ergun, R. E. (2016). Van Allen Probes observations of oxygen cyclotron harmonic waves in the inner magnetosphere. *Geophysical Research Letters*, *43*, 8827–8834. https://doi.org/10.1002/2016GL070233

Young, D. T., Burch, J. L., Gomez, R. G., de Los Santos, A., Miller, G. P., Wilson, P., et al. (2016). Hot plasma composition analyzer for the magnetospheric multiscale mission. *Space Science Reviews*, *199*(1-4), 407–470. https://doi.org/10.1007/s11214-014-0119-6